Rotational spectroscopy and astronomical search for the 2-hydroxyacetonitrile isotopologues (HOCH2CN)-C-13, (HOCH2CN)-C-13, and DOCH2CN

L. Margulès, A. Coutens, N. F. W. Ligterink, A Ahmadi, R.A. Motiyenko, E.A. Alekseev, C. Vastel, E. Caux, J-C Guillemin

Rotational spectroscopy and astronomical search for the 2-hydroxyacetonitrile isotopologues HO^{13}CH$_2$CN, HOCH$_2^{13}$CN and DOCH$_2$CN

L. Margulès,[1]★ A. Coutens,[2] N. F.W. Ligterink,[3] A. Ahmadi,[4] R. A. Motiyenko,[1] E. A. Alekseev,[1,5] C. Vastel,[2] E. Caux,[2] and J.-C. Guillemin[6]

[1] *Univ. Lille, CNRS, UMR 8523 - PhLAM - Physique des Lasers Atomes et Molécules, F-59000 Lille, France*

[2] *Institut de Recherche en Astrophysique et Planétologie (IRAP), Université de Toulouse, UPS-OMP, CNRS, CNES, 9 av. du Colonel Roche, 31028 Toulouse Cedex 4, France*

[3] *Physics Institute, University of Bern, Sidlerstrasse 5, 3012 Bern, Switzerland*

[4] *Leiden Observatory, Leiden University, PO Box 9513, 2300 RA Leiden, The Netherlands*

[5] *Radiospectrometry Department, Institute of Radio Astronomy of NASU, Kharkiv, Ukraine*

[6] *Univ Rennes, Ecole Nationale Supérieure de Chimie de Rennes, CNRS, ISCR UMR6226, F-35000 Rennes, France*

Accepted XXX. Received YYY; in original form ZZZ

ABSTRACT

The main isotopologue of 2-hydroxyacetonitrile (glycolonitrile; HOCH$_2$CN) has recently been detected in the interstellar medium (ISM). To date, no rotational spectroscopy of 2-hydroxyacetonitrile ^{13}C-isotopologues studies has been carried out and only few centimeter-wave measurements of one deuterated isotopologue (DOCH$_2$CN) exist. The rotational spectrum of the 2-hydroxyacetonitrile 13C-isotopologues and DOCH$_2$CN was investigated from 150 to 530 GHz. As the parent isotopic species, the other 2-hydroxyacetonitrile isotopologues exhibit large amplitude motion due to the torsion of the hydroxyl group. The analysis of the spectra were carried out using the RAS formalism and Watson's S-reduction Hamiltonian implemented in the SPFIT code. More than 3000 lines were fitted for the three studied isotopologues, with quantum number values reaching 60 to 67 for J and 21 to 25 for K_a depending on the species. Accurate line lists up to 600 GHz and partition functions are provided. A search for these isotopologues in SMM1-a and IRAS16293 B surveys resulted in non-detections; upper limits to the column density were determined. The accurate spectroscopic prediction of their spectra provided in this work will allow astronomers to continue the search for 2-hydroxyacetonitrile isotopologues in the ISM.

Key words: ISM: molecules – methods: laboratory: molecular – submillimetre: ISM – molecular data – line: identification – astrochemistry

1 INTRODUCTION

The astrochemical study of the isotopologues (or isotopomers) of a molecule detected in the interstellar medium (ISM) is an essential tool for improving the understanding of the formation of these compounds by searching for similar isotopic ratios in possible precursors. This approach thus allows to eliminate a number of potential reactants and the reactions associated with them. The remaining precursor(s) allows considering possible chemical reactions which can also lead to other compounds which become target compounds. On Earth, the ^{13}C/^{12}C ratio is about 1%. This ratio can vary considerably depending on the studied area of the universe. It is of the order of 4 to 5% in the region of the Galactic Center, and 1–2% in the Solar neighborhood (Halfen et al. 2017; Müller et al. 2008; Jacob et al. 2020; Wilson & Rood 1994). Similarly, deuterated compounds were observed. Even trideuterated compounds, ND$_3$ and CD$_3$OH, were detected, this implies a huge enhancement factor compared to the deuterium/hydrogen cosmic value (Roueff et al. 2005; Parise et al. 2004). In order to quantify the ratio between isotopologues, laboratory recording of the spectrum of each isotopologue is necessary before detecting them and determining the ratio between each and the main isotopomer if they are sufficiently abundant to perform such studies. We recently reported the millimeter spectrum of 2-hydroxyacetonitrile (HOCH$_2$CN, glycolonitrile, hereafter hydroxyacetonitrile) (Margulès et al. 2017) and this compound was detected a few months later in both the inner hot corino and the outer cold envelope of IRAS16293 B (Zeng et al. 2019). Later, a second detection of hydroxyacetonitrile was reported towards Serpens SMM1-a (Ligterink et al. 2021). These two detections are thus far the only observations of this molecule. Hydroxyacetonitrile is considered a prebiotic molecule because it is a catalyst for the formation of the nucleobase adenine (Schwartz & Goverde 1982) and is often a byproduct in the synthesis by a Strecker reaction of aminoacetonitrile (NH$_2$CH$_2$CN). It can be formed in the ISM through the reaction of the CN anion or radical with formaldehyde (Danger et al. 2012). Thus, a link can be established between the ratios of the ^{13}C and ^{12}C isotopologues of hydroxyacetonitrile if they are detected, and those of formaldehyde and hydrogen cyanide in the event that such

★ E-mail: laurent.margules@univ-lille.fr

ratios can be measured for these compounds in the same area. We report here the synthesis, measurements, and analysis of the two ^{13}C isotopomers of ($HO^{13}CH_2CN$ and $HOCH_2^{13}CN$) and one deuterated isotopologue ($DOCH_2CN$) spectra in the range 150–530 GHz.

2 EXPERIMENTAL SECTION

2.1 Synthesis

Paraformaldehyde-^{13}C and potassium cyanide-^{13}C were purchased from Eurisotop and used without further purification. Formaldehyde (37 wt % in water), potassium cyanide and methanol-*d* (CH_3OD) were purchased from Sigma-Aldrich. 2-hydroxyacetonitrile-*1*-^{13}C and 2-hydroxyacetonitrile-*2*-^{13}C were prepared as previously reported for the main isotopologue (Gaudry 1947, 1955) but using paraformaldehyde-^{13}C or potassium cyanide-^{13}C, respectively.

Hydroxyacetonitrile-*1*-^{13}C. To obtain 6 g of a 20 wt % aqueous solution of ^{13}C-formaldehyde, paraformaldehyde-^{13}C (1.20 g) was diluted in water (4.8 g) under stirring, heating to 50°C and then cooled at room temperature. In a 50 mL flask cooled to 0°C, potassium cyanide (2.6 g, 40 mmol) was dissolved in water (5 mL) and formaldehyde-^{13}C (20% in water, 6 g) was added dropwise. After 10 min standing, 4.6 mL of dilute sulfuric acid (1.14 mL, 1.84 g/ml, in 3.5 ml of water) was added dropwise to the cold solution (0°C). A copious precipitate of potassium sulfate was formed. The pH of the solution was about 1.9. A 10% potassium hydroxide solution was then added, dropwise, and with cooling, until the pH was about 3.0. The flask was then removed from the cooling bath, 10 mL of diethyl ether have been added, and the mixture was well shaken. The salt was removed by filtration, and washed with 5 mL of diethyl ether. 2-hydroxyacetonitrile-*1*-^{13}C was then extracted (10 x10 mL of diethyl ether), dried and distilled in vacuo. Yield: 65%. ^{1}H NMR (CD_3CN, 400 MHz) δ 3.83 (m brd, 1H, OH); 4.29 (dd, 2H, $^1J_{CH}$ = 152.6 Hz, $^3J_{HH}$ = 6.4 Hz, CH_2). ^{13}C NMR (CD_3CN, 100 MHz) δ 48.1 ($^1J_{CH}$ = 152.6 Hz (t), CH_2); 118.7 (d, $^1J_{CC}$ = 59.5 Hz (d), CN).

Hydroxyacetonitrile-*2*-^{13}C. The same procedure was used with potassium cyanide-^{13}C (2.7 g, 40 mmol), water (5 mL) and formaldehyde (3.4 mL, 37 wt % in water and 2.6 mL of water). Yield: 65%. ^{1}H NMR (CD_3CN, 400 MHz) δ 3.83 (m brd, 1H, OH); 4.29 (dd, 2H, $^2J_{CH}$ = $^3J_{HH}$ = 6.4 Hz, CH_2). ^{13}C NMR (CD_3CN, 100 MHz) δ 48.1 ($^1J_{CC}$ = 59.5 Hz (d), $^1J_{CH}$ = 152.6 Hz (t), CH_2); 118.7 ($^2J_{CH}$ = 6.4 Hz (t), CN).

Deuteroxyacetonitrile. Methanol-*d* CH_3OD (3.2 g, 0.1 mol) was added to hydroxyacetonitrile (1.14 g, 20 mmol) and the mixture was stirred for 10 min at room temperature. Low boiling compounds were removed in vacuo and the reaction repeated twice.

2.2 Lille: Submillimeter wave spectra

The measurements in the frequency range under investigation (150–530 GHz) were performed using the Lille spectrometer (Zakharenko et al. 2015). The absorption cell was a stainless-steel tube (6 cm in diameter, 220 cm in length). The sample pressure and temperature during measurements were about 10 Pa and room temperature, and the line width was limited by Doppler broadening. The frequency range 150–530 GHz was covered with various active and passive frequency multipliers from VDI Inc. and an Agilent synthesizer (12.5–18.25 GHz) was used as the source of radiation. Absorption signals were detected by an InSb liquid He-cooled bolometer (QMC Instruments Ltd.). Estimated uncertainties for measured line frequencies are 30 kHz and 50 kHz depending on the observed S/N and the frequency range.

3 ANALYSIS OF THE ROTATIONAL SPECTRA

As for the parent isotopic species, we only analyzed the spectra of the *gauche* rotamer, which is the most stable one. The *trans* rotamer of hydroxyacetonitrile is calculated to be 1.41 kcal.mol^{-1} (493 cm^{-1}/710 K) higher in energy (Dalbouha et al. 2017). The analysis was complicated by a large amplitude motion (LAM) with a symmetric two minima potential due to the two equivalent *gauche* rotamers. As a result of the tunneling through the barrier to OH-group torsion, each energy level of 2-hydroxyacetonitrile is split into two substates labeled here as 0 (the lowest energy level) and 1. The corresponding labeling used by Dalbouha et al. (2017) is A1 and A2. The structure of *gauche* rotamer is very close to a symmetric prolate rotor with an asymmetry parameter κ = -0.968. Many nitriles are characterized by large dipole moment. It is also the case of 2-hydroxyacetonitrile: μ_a = 2.32 D, μ_b = 1.31 D, μ_c = 1.23 D. These ab initio values are from Dalbouha et al. (2017). It should be noted that the component of the dipole moment along *c*-axis is linked to torsion motion, and allows transitions between the two torsional substates.

For the global fit, a model based on the reduced axis system (RAS) approach proposed by Pickett (1972) was implemented in the widely used SPFIT/SPCAT programs for fitting and predicting molecular spectra. Is has been shown by Christen & Müller (2003) that the RAS formalism is equivalent to the internal-axis-method (IAM) approches developed by Hougen and coworkers for molecules with several large amplitude motions (Hougen 1985; Coudert & Hougen 1988). This method is particulary suitable for double minimum LAM cases, we employed it successfully in previous studies (Motiyenko et al. 2010; Smirnov et al. 2013; Motiyenko et al. 2015) and in particular with the hydroxyacetonitrile normal species (Margulès et al. 2017). More details about the model can be found in this paper.

3.1 ^{13}C isotopologues

The analysis of the ^{13}C isotopologues was rather straightforward. Even if no spectroscopic studies existed up to now, we could take benefit of the main isotopologue study. Substituting the ^{12}C with ^{13}C does not affect significantly kinetic and potential energy of LAM as it can be verified in the final parameters set table (Table 1). With this assumption, for both ^{13}C isotopologues, we used as starting parameters the *ab initio* ground vibrational state rotational constants of Table 2 in Dalbouha et al. (2017) while all the other parameters (centrifugal distortion, tunneling splitting, and Coriolis coupling constants) were taken from Margulès et al. (2017). The initial predictions obtained using these parameters allowed, for example, easy assignment of $HO^{13}CH_2CN$ ^aR-branch J = 17 − 16 band heads at 156 GHz that were shifted by 260 MHz in the experimental spectrum. The ^aR branch transitions are the most intense in the spectra, due to the large μ_a value. Their assignment and improvement of the set of Hamiltonian parameters permitted the search for *b*-type transitions. Finally, we were also able to assign *c*-type transitions connecting two torsional substates. Going step by step with the different ranges (150-220, 225-330, 400-530 GHz) permitted to determine almost all the rotational and tunneling parameters we could fit in the main isotopologue study (Margulès et al. 2017). The same procedure was used for the second ^{13}C isotopologue: $HOCH_2^{13}CN$. Some of the octic distorsion constants which could not be determined better than 10 times

their standard deviation were kept fixed at the main isotopologue values.

In total, 3403 distinct lines of the $HO^{13}CH_2CN$ isotopologue were assigned with maximum values for J and K_a of 67 and 25, respectively. The standard deviation of the fit is 26.3 kHz and 45 parameters were determined. For $HOCH_2^{13}CN$ isotopologue, the dataset is composed of 3235 lines with maximum values for J and K_a of 63 and 26, respectively. The standard deviation of the fit is 28.7 kHz and 44 parameters were determined. The number of parameters needed to reproduce experimental accuracy seems important, but this is generally the case when dealing with large amplitude motion.

The final set of parameters that we obtained are listed in Table 1. The first column of the table shows the parameters of the main isotopologue from Margulès et al. (2017). This permits to check the good agreement of the ^{13}C parameters from this new study with the ^{12}C ones. From the analysis of Table 1, it can be clearly seen that ^{12}C to ^{13}C isotopic substitution has a very limited influence on tunneling Hamiltonian parameters. We also compare in Table 2 the rotational constants A, B, and C, and energy difference between tunneling sublevels E from our study with the *ab initio* calculations. The difference between theoretical and experimental values for ^{13}C isotopologues have the same order of magnitude as for the main isotopologue (see Table 2 of Margulès et al. (2017)). This confirms the quality of the results obtained in this work.

3.2 Deuterated isotopologue: $DOCH_2CN$

Despite the existence of centimeter-wave measurements (Cazzoli et al. 1973), the analysis of the $DOCH_2CN$ spectra was more complicated. The deuteration of the hydroxyl group hydrogen implies a significant variation of the mass of the tunneling atom which has a direct influence on the tunneling probability and hence on the splitting between 0 and 1 substates, and in general, on the tunneling dynamics. Therefore, for $DOCH_2CN$ isotopic species, as starting set of tunneling and Coriolis coupling parameters, we could not use the ones determined for the parent or ^{13}C species. The initial assignment and analysis were performed separately for the two tunneling substates. The initial spectral predictions were calculated with Watson's Hamiltonian in the I^r representation, the rotational parameters from Cazzoli et al. (1973), and the *ab initio* quartic centrifugal distortion constants (Dalbouha et al. 2017). In such manner we assigned ^aR-branch transitions for both substates up to $K"_a = 4$ in the 150–300 GHz range corresponding to $J"$ between 18 and 30. The assignment of higher K_a transitions was not possible without taking Coriolis-type interaction between tunneling substates into account. However, the least-squares fitting using the global model is not straightforward due to the strong correlation between tunneling and Coriolis-coupling parameters. In this case, the initial fit strategy is to fix one of the two parameters, the energy difference E or the Coriolis coupling parameter F_{bc}, to a series of reasonable values, to vary the second one, and to search for a minimum rms deviation solution as a function of fixed parameter Motiyenko et al. (2018). We used E as fixed parameter in the range between 15 and 18 GHz that comprises the corresponding values from *ab initio* calculations, 15.3 GHz, and from an estimation by Cazzoli et al. (1973), 16.7 GHz. Using this strategy, the minimum rms deviation fit was obtained for $E = 17.5$ GHz. New predictions calculated using optimized value of E allowed us to locate and assign in the spectra c-type transitions that connect two tunneling substates, and thus, to remove the correlation between tunneling and Coriolis-coupling parameters. One should note that without accurate estimation of E, it is almost impossible to assign correctly c-type transitions. For example, the c-type transition frequencies calculated using E values from Dalbouha et al. (2017) or Cazzoli et al. (1973) are shifted by few GHz compared to experimental positions. Finally, after removing the correlations, we switched to a model that uses a single set of rotational and centrifugal distortion parameters for both substates, as in the case of the parent or ^{13}C isotopic species.

A total of 3190 distinct lines of the $DOCH_2CN$ were assigned with maximum values for J and K_a of 60 and 21, respectively. Among the assigned lines 393 lines are transitions between tunneling substates. 44 parameters were determined and the standard deviation of the fit is 26.6 kHz. We can observe in the Table 2 a good agreement of the rotational constants and energy difference of the sublevels from our study with the *ab initio* calculations. As mentioned for ^{13}C species, the difference observed have the same order of magnitude as the main isotopologue (Margulès et al. 2017). For example, the energy difference we obtained 17567.061(10) MHz is in good agreement with 15289.4 MHz, regarding the 15% accuracy for the main and ^{13}C isotopologues.

Part of the new measurements with the fit residuals for $HO^{13}CH_2CN$, $HOCH_2^{13}CN$ and $DOCH_2CN$ are given in Tables 3, 4 and 5. Owing to their large size, the complete versions of the global fit (Tables S1, S2 and S3) for the three isotopologues are supplied at the CDS[1]. The predicted spectra are available in different formats including standard .cat format (Pickett 1972) from the new database of the Lille spectroscopy group called the Lille Spectroscopic Database[2]. The predictions can be generated using various options (e.g., intensity units, temperature, and frequency range) that provide additional flexibility in the data access.

3.3 Partition function

The tabulated values for the partition function are given in Table 6, with $Q_{tot}(T) = Q_{vib}(T) \times Q_{rot}(T)$. The rotational partition function was obtained directly at various temperatures from SPCAT (Pickett 1991) with J up to 90, and K_a up to 40. The vibrational contribution was calculated in the harmonic approximation (Gordy et al. 1984), as we proceeded in our previous studies (see, e.g., Margulès et al. 2020). The four lowest vibrational excited states levels were considered. The remaining ones above 870 cm^{-1} (1252 K) were found to have no influence on the partition function calculations especially at temperatures below 200 K. The band centers values were taken from Table 3 in Dalbouha et al. (2017).

4 ASTRONOMICAL OBSERVATIONS: SEARCH FOR HYDROXYACETONITRILE ISOTOPOLOGUES IN SMM1-A AND IRAS16293 B

4.1 SMM1-a

The main isotopologue of hydroxyacetonitrile has been detected towards Serpens SMM1-a (hereafter SMM1-a) at high abundance (Ligterink et al. 2021), making this a suitable target to search for its isotopologues $DOCH_2CN$, $HO^{13}CH_2CN$ and $HOCH_2^{13}CN$. The source, observations, and methods are described in Ligterink et al. (2021) and therefore be covered briefly here. SMM1 is a well characterized and chemically rich source, located at a distance of 436±10 pc (Ortiz-León et al. 2017), and consists of multiple protostars. The brightest, SMM1-a, is an intermediate-mass Class 0 protostar. Recently, this source was targeted with ALMA towards a phase centre

[1] https://cds.unistra.fr
[2] https://lsd.univ-lille.fr

Table 1. Spectroscopic parameters of the ^{13}C and deuterated gauche conformer of 2-hydroxyacetonitrile species

Parameters in MHz	$HOCH_2CN^a$	$HO^{13}CH_2CN$	$HOCH_2^{13}CN$	$DOCH_2CN$
		Rotational and centrifugal distortion constants		
A	33609.53194(27)^b	32787.31228(29)	33569.30468(40)	30653.94661(70)
B	4838.014347(41)	4820.980595(68)	4810.878790(83)	4725.725505(99)
C	4377.304462(40)	4349.083437(65)	4354.399428(80)	4262.86028(24)
$D_J * 10^3$	3.093051(44)	3.008971(76)	3.049000(80)	3.280413(94)
$D_{JK} * 10^3$	-63.89803(34)	-59.85131(51)	-64.23275(47)	-54.586(17)
$D_K * 10^3$	969.2208(61)	917.8160(52)	982.3170(80)	753.258(32)
$d_1 * 10^3$	-0.695725(10)	-0.692148(22)	-0.685525(26)	-0.788049(46)
$d_2 * 10^3$	-0.041757(18)	-0.043740(23)	-0.040349(15)	-0.055228(45)
$H_J * 10^6$	0.0107392(81)	0.010232(23)	0.010513(28)	0.011381(31)
$H_{JK} * 10^6$	-0.16090(71)	-0.1265(13)	-0.17990(54)	0.2101(91)
$H_{KJ} * 10^6$	-3.6005(17)	-3.4904(44)	-3.4713(15)	-5.399(33)
$H_K * 10^6$	82.883(56)	77.670(30)	83.883(55)	60.75(11)
$h_1 * 10^6$	0.0044035(40)	0.004285(11)	0.004305(13)	0.004613(22)
$h_2 * 10^6$	0.0005288(27)	0.0005242(20)	0.0005086(18)	0.000368(11)
$h_3 * 10^6$	0.00007335(95)	0.0000622(12)	0.00008221(61)	
$L_K * 10^9$	-3.14(17)	-3.14^c	-3.14^c	
$L_{KKJ} * 10^9$	0.3292(25)	0.3028(20)	0.3435(15)	0.751(18)
$L_{JK} * 10^9$	-0.04864(29)	-0.04450(42)	-0.04609(63)	0.000169(33)
$L_{JJK} * 10^9$	0.001496(12)	0.001417(24)	0.001485(27)	-0.1871(34)
$L_J * 10^9$	-0.00005190(75)	-0.0000553(28)	-0.0000624(36)	-0.0000840(34)
$l_1 * 10^9$	-0.00002619(46)	-0.0000298(16)	-0.0000265(19)	-0.0000208(26)
$l_2 * 10^9$	-0.00000544(39)	-0.00000544^c	-0.00000544^c	
$l_3 * 10^9$	-0.00000236(17)	-0.00000236^c	-0.00000236^c	
		Tunneling splitting constants		
E	112672.5526(30)	112016.5779(41)	112716.4480(55)	17567.0493(89)
E_J	1.0954348(39)	1.0751770(59)	1.0883325(56)	0.380161(59)
E_K	-13.606157(53)	-13.273996(71)	-13.78242(11)	-3.71749(19)
$E_{JJ} * 10^3$	-0.00749(11)	-0.00487(24)	-0.01055(13)	-0.007934(35)
$E_{JK} * 10^3$	-0.19132(72)	-0.2154(14)	-0.16000(80)	-0.1601(30)
$E_{KK} * 10^3$	0.44739(78)	0.4516(14)	0.3688(14)	0.1017(35)
E_2	0.331606(22)	0.329474(47)	0.329718(27)	0.119585(35)
$E_{2J} * 10^3$	-0.0073918(30)	-0.0072687(69)	-0.0073022(88)	-0.005092(24)
$E_{2K} * 10^3$	1.339(22)	1.589(46)	0.664(26)	0.3930(43)
$E_{2JJ} * 10^9$	0.07826(71)	0.0935(16)	0.0928(19)	0.1222(28)
$E_{2JK} * 10^9$	-21.80(20)	-19.53(34)	-29.19(32)	-18.93(28)
$E_4 * 10^6$	-5.215(60)	-6.29(12)	-3.533(63)	-1.8968(74)
$E_{4J} * 10^9$	0.1756(13)	0.1959(27)	0.2005(28)	0.2708(34)
		Coriolis coupling constants		
F_{bc}	-5.7926(14)	-5.9589(18)	-5.77100(11)	-3.32962(35)
$F_{bcK} * 10^3$	43.41(74)	56.41(92)	31.77(59)	-112.97(28)
$F_{bcJ} * 10^3$	-0.113411(86)	-0.115675(85)	-0.11216(10)	-0.46075(94)
$F_{bcKK} * 10^6$	-19.08(43)	-12.27(24)	-25.60(32)	38.69(80)
$F_{bcJK} * 10^6$	0.4789(72)	0.3470(77)	0.517(11)	
$F_{bcJJ} * 10^6$				0.014149(81)
$F_{2bc} * 10^6$	86.5(14)	116.7(19)	62.3(11)	-22.135(52)
F_{ac}	75.52596(18)	73.71299(25)	75.01253(25)	136.707(18)
$F_{acJ} * 10^3$	-0.05771(28)	-0.07313(36)	-0.05196(44)	
$F_{acK} * 10^3$	9.943(25)	10.099(30)	9.835(36)	19.91(91)
$F_{acJK} * 10^6$	0.485(16)	0.185(16)	0.193(16)	
$F_{acKK} * 10^6$	-9.229(30)	-8.740(29)	-8.798(37)	-34.37(42)
Number of distincts lines	5128	3403	3235	3190
Number of parameters	47	45	44	44
$J''_{max}, K''_{a,max}$	75, 25	67, 25	63,26	60,21
Standard deviation (in kHz)	29.2	26.3	28.7	26.3
Weighted deviation	0.931	0.855	0.916	0.875

[a] Margulès et al. (2017); [b] Number in parentheses is one standard deviation in unit of the last digit; [c] Fixed to main isotopologue value

of α_{J2000} = 18:29:49.80, δ_{J2000} = +01:15:20.6. Selected frequency windows in Band 6 between 217 and 235 GHz were targeted. A synthetic beam of approximately 1.2" was employed, which is insufficient to resolve the hot corino. Analysis of an extracted spectrum towards the SMM1-a continuum peak in a single beam with the CASSIS[3] line analysis software resulted in the detection of sev-

[3] Based on analysis carried out with the CASSIS software (http://cassis.irap.omp.eu; (Vastel et al. 2015) and JPL database for molecular spectroscopy (Pickett et al. 1998) and the Cologne Database for

Table 2. Comparison of experimental and ab initio parameters in MHz

Parameters	$HO^{13}CH_2CN$		$HOCH_2^{13}CN$		$DOCH_2CN$		
	this work	ab initio[a]	this work	ab initio	this work	ab initio	Cazzoli et al.[c]
A	32787.31523(44)[b]	32800.04	33569.30468(40)	33579.15	30653.94661(70)	30666.47	30651.04(22)
B	4820.980561(79)	4811.81	4810.878790(83)	4801.98	4725.725505(99)	4716.15	4726.75(22)
C	4349.083413(75)	4342.59	4354.399428(80)	4348.01	4262.86028(24)	4255.64	4262.36(22)
E	112016.5659(48)	95334.00	112716.4480(55)	96533.17	17567.061(10)	15.289.42	16749.57

[a] Dalbouha et al. (2017); [b] Number in parentheses is one standard deviation in unit of the last digit; [c] Cazzoli et al. (1973)

Table 3. Measured frequencies of the $HO^{13}CH_2CN$ isotopologue and residuals from the fit (full fit is available at the CDS: S1)

Upper level				Lower level				Frequency(Unc.)	o.-c.
J"	K_a"	K_c"	v_t"a	J'	K'_a	K'_c	v'^a_t	(in MHz)	(in MHz)
61	1	60	1	60	1	59	1	539819.787(0.030)	-0.000
61	2	60	1	60	1	59	1	539863.767(0.030)	0.004
60	3	58	1	59	2	57	1	539875.463(0.030)	-0.031
61	1	60	0	60	2	59	0	539908.910(0.030)	-0.009
19	7	12	0	18	6	13	0	539943.488(0.030)	0.002
19	7	13	0	18	6	12	0	539943.488(0.030)	0.030
61	2	60	0	60	2	59	0	539950.533(0.030)	-0.042
61	1	60	0	60	1	59	0	539959.986(0.030)	-0.002
58	4	54	1	57	4	53	1	539974.592(0.030)	0.040
60	3	58	0	59	2	57	0	539977.449(0.030)	-0.030

[a] following SPFIT format the torsional substates $A1$ and $A2$ are labeled 0 and 1, respectively

Table 4. Measured frequencies of the $HOCH_2^{13}CN$ isotopologue and residuals from the fit (full fit is available at the CDS: S2)

Upper level				Lower level				Frequency(Unc.)	o.-c.
J"	K_a"	K_c"	v_t"a	J'	K'_a	K'_c	v'^a_t	(in MHz)	(in MHz)
45	5	40	0	44	4	40	1	527413.846(0.03000)	-0.032
33	3	30	1	32	2	30	0	527665.846(0.03000)	0.079
52	4	49	1	51	3	48	1	527765.891(0.03000)	0.036
58	4	55	1	57	4	54	1	528239.640(0.03000)	-0.001
58	4	55	0	57	4	54	0	528436.677(0.03000)	0.042
56	8	49	1	56	7	49	0	528606.153(0.03000)	-0.063
17	5	12	1	16	4	12	0	528611.553(0.03000)	-0.023
17	5	13	1	16	4	13	0	528642.147(0.03000)	-0.056
23	6	17	0	22	5	18	0	528776.749(0.03000)	0.047
23	6	17	1	22	5	18	1	528984.733(0.03000)	0.057

[a] following SPFIT format the torsional substates $A1$ and $A2$ are labeled 0 and 1, respectively

Table 5. Measured frequencies of the $DOCH_2CN$ isotopologue and residuals from the fit (full fit is available at the CDS: S3)

Upper level				Lower level				Frequency(Unc.)	o.-c.
J"	K_a"	K_c"	v_t"a	J'	K'_a	K'_c	v'^a_t	(in MHz)	(in MHz)
20	7	13	0	19	6	14	0	519153.053(0.03000)	-0.021
20	7	14	0	19	6	13	0	519153.053(0.03000)	0.044
20	7	13	1	19	6	14	1	519208.530(0.03000)	-0.064
20	7	14	1	19	6	13	1	519208.530(0.03000)	0.000
30	5	26	1	29	4	26	0	519570.812(0.03000)	-0.001
24	6	18	1	23	5	18	0	519677.999(0.03000)	0.033
24	6	19	1	23	5	19	0	519704.748(0.03000)	0.066
57	4	53	1	56	4	52	1	519765.867(0.03000)	0.024
57	4	53	0	56	4	52	0	519853.924(0.03000)	-0.079
56	4	53	1	55	3	52	1	519863.089(0.03000)	0.012
59	3	57	0	58	2	56	0	519888.201(0.03000)	0.026

[a] following SPFIT format the torsional substates $A1$ and $A2$ are labeled 0 and 1, respectively

Table 6. Rotational, vibrational, and total partition functions of 2-hydroxyacetonitrile isotopologues at various temperatures.

	$HO^{13}CH_2CN$			$HOCH_2^{13}CN$			$DOCH_2CN$		
T (K)	Q_{rot}(T)	Q_{vib}(T)	Q_{tot}(T)[a]	Q_{rot}(T)	Q_{vib}(T)	Q_{tot}(T)[a]	Q_{rot}(T)	Q_{vib}(T)	Q_{tot}(T)[a]
300	66349.366	2.945	195427.600	65599.953	2.983	195705.692	70508.718	3.448	243084.660
225	43025.987	1.938	83402.987	42538.671	1.955	83169.251	45852.122	2.201	100939.594
150	23269.950	1.316	30624.476	23005.366	1.321	30395.412	24923.049	1.428	35588.472
75	8080.026	1.028	8303.656	7987.232	1.028	8212.221	8781.574	1.047	9198.324
37.5	2762.515	1.000	2763.682	2730.231	1.000	2731.423	3088.620	1.001	3092.371
18.75	917.588	1.000	917.588	906.545	1.000	906.545	1081.656	1.000	1081.657
9.375	290.775	1.000	290.775	287.126	1.000	287.126	375.515	1.000	375.515

[a] Q_{tot}(T) values are calculated without truncation of Q_{rot}(T) and Q_{vib}(T) at the third digit

eral prebiotic molecules, including $HOCH_2CN$. Hydroxyacetonitrile was detected at N_{Tot} = (7.4±0.9)×10^{14} cm^{-2}, T_{ex} = 260±45 K, ΔV 2.5±0.3 km.s^{-1}, and V_{LSR} = 6.8±0.2 km.s^{-1} (Ligterink et al. 2021). To identify the isotopologues, their lines are searched within a 3 S/N detection. Upon identification, a synthetic spectrum is fitted to these lines, assuming Local Thermodynamic Equilibrium (LTE) conditions. If no lines are detected, the upper limit column density of an isotopologue is determined in line-free spectral regions where a transition of said isotopologue is located. The parameters T_{ex}, ΔV, and V_{LSR} are adopted from the main isotopologue. In the SMM1-a spectra, the three hydroxyacetonitrile isotopologues are not detected. Several of their undetected transitions are presented in Figures 1, 2, 3, for $DOCH_2CN$, $HO^{13}CH_2CN$ and $HOCH_2^{13}CN$, respectively. Due to the line-richness of the spectrum, it is difficult to find completely line free spectral regions. For $HO^{13}CH_2CN$, blended line features seem to be present in the observed spectrum, but these can both be attributed to CH_3COOH. The $26_{2,25} \leftarrow 25_{2,24}$ transition of the synthetic $HOCH_2^{13}CN$ spectrum blends in the wing with a CH_3CDO line in the observed spectrum. Due to the issues in determining line free spectral regions, a conservative estimate of the upper limit column density is given. For $DOCH_2CN$ $N_{tot} \leq 1 \times 10^{14}$ cm^{-2}, while for both ^{13}C isotopologues it is set a $N_{tot} \leq 2 \times 10^{14}$ cm^{-2}. This results in [isotopologue]/[$HOCH_2CN$] ratios of $\leq$ 0.14 and $\leq$ 0.27 for the deuterated and ^{13}C hydroxyacetonitrile isotopologues, respectively. Part of the reason that the isotopologues of $HOCH_2CN$ are not detected lies in the fact that the spectral windows of the SMM1-a observations miss the most of the strongest transitions of these species. Figure 4 shows the normalized synthetic spectra of $DOCH_2CN$, $HO^{13}CH_2CN$ and $HOCH_2^{13}CN$ at T_{ex} = 260 K, with the location of the spectral windows indicated. Only several $DOCH_2CN$ lines are covered in the low resolution continuum band between 234.06 and 235.93 GHz. Follow-up observations with ALMA that target the strongest isotopologue transition at higher sensitivity will presumably be more successful in detecting these species.

4.2 IRAS16293 B

$HOCH_2CN$ has also been detected towards the low-mass protostar IRAS16293 B (Zeng et al. 2019; Ligterink et al. 2021). Contrary to SMM1-a, a large spectral range (329–363 GHz) has been covered for this source in the framework of the ALMA-PILS survey, which is fully described in Jørgensen et al. (2016). Faint lines of hydroxyacetonitrile lines were identified at the so-called half-beam offset position (Ligterink et al. 2021). We consequently searched for the ^{13}C isotopologues at the same position. No lines of the ^{13}C isotopologues are detected. Assuming an excitation temperature of 150 K (similar to the one obtained by Zeng et al. 2019), a source size of 0.5″, a linewidth ΔV = 1 km s^{-1}, and a V_{LSR} = 2.7 km.s^{-1}, we derive an upper limit of 1.5×10^{15} cm^{-2} for both $HO^{13}CH_2CN$ and $HOCH_2^{13}CN$. The upper limit would be lower if the excitation temperature is higher. Using the column density of 3×10^{15} cm^{-2} derived for the main isotopologue by Ligterink et al. (2021), we obtain a $^{13}C/^{12}C \leq 0.5$. $DOCH_2CN$ was also searched for in the PILS survey but is undetected with a column density lower than 1.5×10^{15} cm^{-2} for T_{ex} = 150 K. This leads to an upper limit for the D/H ratio of 50%, which is well above the values derived for the mono-deuterated isotopologues of other complex organic molecules in this source with the same survey: 1-8% (Coutens et al. 2016, 2018; Jørgensen et al. 2018; Persson et al. 2018; Müller et al. 2023). Given the lower constraints obtained for IRAS16293 B and the small spectral range covered by the observations of SMM1-a so far, it appears that SMM1-a would be a better target for follow-up observations.

Table 7. Derived isotopic ratios towards IRAS16293B and SMM1-a.

Source	SMM1-a	IRAS16293B
$^{13}C/^{12}C$	$\lesssim$ 0.27	$\lesssim$ 0.5
D/H	$\lesssim$ 0.14	$\lesssim$ 0.5

As Zeng et al. (2019) identified clearer lines of $HOCH_2CN$ towards IRAS16293 B with larger angular resolution observations, we also checked the ALMA archive data with angular sizes between 1 and 2″. We used the ATOMIS[4] web application to search for the three isotopologues in the archival ALMA data with the following request: an angular resolution between 1 and 2 ″, a spectral resolution better than 0.5 km s^{-1}, and a sensitivity better than 6 mJy beam^{-1} for a bin width of 1 km s^{-1}. We restricted the search to the Bands 3, 4, 5, and 6 similarly to Zeng et al. (2019) and we only looked at the transitions with an A_{ij} higher than 5 × 10^{-5} s^{-1}. We found that one transition of $HOCH_2^{13}CN$ and two transitions of $HO^{13}CH_2CN$ at 139.5831, 139.6833, and 139.8175 GHz, respectively, are covered in the project 2013.1.00352.S. Multiple transitions of $DOCH_2CN$ are covered in the project 2018.1.01496.S. We visualize the fits cubes provided on the ALMA archive with Aladin[5] and CASSIS. The $HOCH_2^{13}CN$ line at 139.5831 GHz is blended with a CH_3COCH_3 line. The two transitions of $HO^{13}CH_2CN$ are within the noise. No

Molecular Spectroscopy (Müller et al. 2001, 2005; Endres et al. 2016). CASSIS has been developed by IRAP-UPS/CNRS.

[4] ATOMIS (ALMA archive Tool for Molecular Investigations in Space) is developed at IRAP-UPS/CNRS in the framework of the ERC starting grant Chemtrip (grant agreement No 949278)

[5] https://aladin.u-strasbg.fr/AladinDesktop/

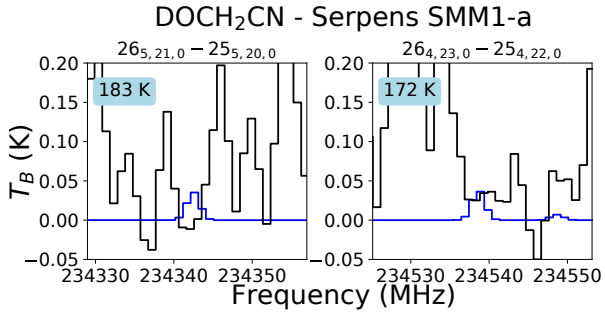

Figure 1. ALMA spectrum of SMM1-a (black) and a synthetic spectrum of $DOCH_2CN$ (blue). Two undetected and largely unblended transitions are shown from which the upper limit column density of $\leq 1{\times}10^{14}$ cm^{-2} is determined. Other synthetic spectrum parameters are adopted from the main isotopologue $HOCH_2CN$ detection towards SMM1-a and are fixed at T_{ex} = 260 K, ΔV = 2.5 km.s^{-1}, and V_{LSR} = 6.8 km.s^{-1}. The upper state energy of each transition is indicated in the top left corner.

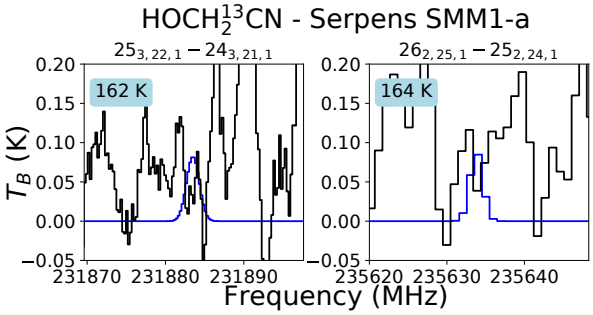

Figure 2. ALMA spectrum of SMM1-a (black) and a synthetic spectrum of $HOCH_2^{13}CN$ (blue). Two undetected and largely unblended transitions are shown from which the upper limit column density of $\leq 2{\times}10^{14}$ cm^{-2} is determined. Other synthetic spectrum parameters are adopted from the main isotopologue $HOCH_2CN$ detection towards SMM1-a and are fixed at T_{ex} = 260 K, ΔV = 2.5 km.s^{-1}, and V_{LSR} = 6.8 km.s^{-1}. The upper state energy of each transition is indicated in the top left corner. The $26_{2,25}$ â $25_{2,24}$ transition is blended in the wing with a CH_3CDO transition.

$DOCH_2CN$ line is detected either. This confirms that SMM1-a could be a better target for future studies.

5 CONCLUSION

Millimeter and submillimeter wave spectra of three 2-hydroxyacetonitrile isotopologues, $HO^{13}CH_2CN$, $HOCH_2^{13}CN$ and $DOCH_2CN$, were assigned up to 530 GHz. This has allowed us to produce accurate predictions of the spectra and made possible a search for these isotopologues in the ISM. Only non-detections could be reported in this work toward SMM1-a and IRAS16293 B with no significant constraints on the $^{13}C/^{12}C$ and D/H ratios of this molecule. The spectroscopic predictions are now available to the astrophysical community, enabling future searches for these 2-hydroxyacetonitrile isotopologues as more sensitive surveys become available.

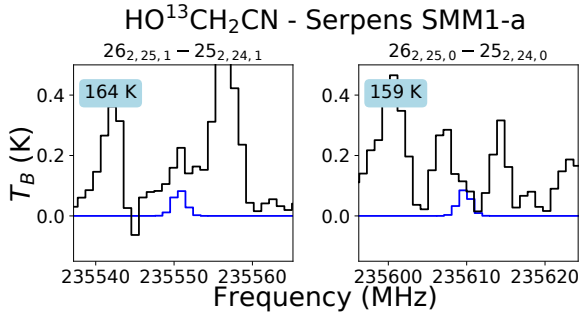

Figure 3. ALMA spectrum of SMM1-a (black) and a synthetic spectrum of $HO^{13}CH_2CN$ (blue). Two undetected and largely unblended transitions are shown from which the upper limit column density of $\leq 2 \times 10^{14}$ cm^{-2} is determined. Other synthetic spectrum parameters are adopted from the main isotopologue $HOCH_2CN$ detection towards SMM1-a and are fixed at T_{ex} = 260 K, ΔV = 2.5 km.s^{-1}, and V_{LSR} = 6.8 km.s^{-1}. The upper state energy of each transition is indicated in the top left corner. Both transitions are blended with CH_3COOH lines.

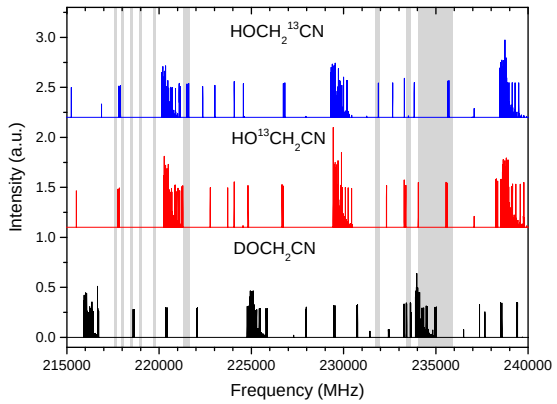

Figure 4. Normalized synthetic spectra of $HOCH_2^{13}CN$ (blue), $HO^{13}CH_2CN$ (red), and $DOCH_2CN$ (black) for T_{ex} = 260 K, ΔV = 2.5 km.s^{-1}, and V_{LSR} = 6.8 km.s^{-1} together with the locations of the spectral windows of the SMM1-a observations (grey). With the exception of a number of $DOCH_2CN$ lines covered by the continuum window, the strongest and most prominent transitions of these hydroxyacetonitrile isotopologues are not covered by the observations.

ACKNOWLEDGEMENTS

This work was supported by the CNRS through the MITI interdisciplinary programs. A.C. received financial support from the European Research Council (ERC) under the European Unions Horizon 2020 research and innovation programme (ERC Starting Grant Chemtrip, grant agreement No 949278). J.C.G. thanks the Centre National d'Etudes Spatiales (CNES) for a grant. N.F.W.L. acknowledges funding by the Swiss National Science Foundation Ambizione grant 193453. This paper makes use of the following ALMA data: ADS/JAO.ALMA2013.1.00278.S, ADS/JAO.ALMA2018.1.00836.S and ADS/JAO.ALMA2013.1.00352.S. ALMA is a partnership of ESO (representing its member states), NSF (USA) and NINS (Japan), together with NRC (Canada), NSC and ASIAA (Taiwan), and KASI (Republic of Korea), in cooperation with the Republic

of Chile. The Joint ALMA Observatory is operated by ESO, AUI/NRAO and NAOJ

DATA AVAILABILITY

Owing to their large size, the complete versions of the global fit (Tables S1, S2 and S3) for the three isotopologues are supplied at the CDS[6]. The predicted spectra are available in different formats including standard .cat format (Pickett 1972) from the new database of the Lille spectroscopy group called the Lille Spectroscopic Database[7].

REFERENCES

Cazzoli G., Lister D., Mirri A., 1973, Journal of the Chemical Society, Faraday Transactions 2: Molecular and Chemical Physics, 69, 569
Christen D., Müller H. S., 2003, Physical Chemistry Chemical Physics, 5, 3600
Coudert L., Hougen J., 1988, Journal of Molecular Spectroscopy, 130, 86
Coutens A., et al., 2016, A&A, 590, L6
Coutens A., et al., 2018, A&A, 612, A107
Dalbouha S., Domínguez-Gómez R. M., Senent M. L., 2017, The European Physical Journal D, 71
Danger G., Duvernay F., Theulé P., Borget F., Chiavassa T., 2012, ApJ, 756, 11
Endres C. P., Schlemmer S., Schilke P., Stutzki J., Müller H. S., 2016, Journal of Molecular Spectroscopy, 327, 95
Gaudry R., 1947, Organic Syntheses, 27, 41
Gaudry R., 1955, Organic Syntheses, 3, 436
Gordy W., Cook R. L., Weissberger A., 1984, Microwave molecular spectra. Vol. 18, Wiley New York
Halfen D. T., Woolf N. J., Ziurys L. M., 2017, ApJ, 845, 158
Hougen J. T., 1985, Journal of Molecular Spectroscopy, 114, 395
Jacob A. M., Menten K. M., Wiesemeyer H., Güsten R., Wyrowski F., Klein B., 2020, A&A, 640, A125
Jørgensen J. K., et al., 2016, A&A, 595, A117
Jørgensen J. K., et al., 2018, A&A, 620, A170
Ligterink N. F. W., et al., 2021, A&A, 647, A87
Margulès L., McGuire B. A., Senent M. L., Motiyenko R. A., Remijan A., Guillemin J. C., 2017, A&A, 601, A50
Margulès L., McGuire B. A., Evans C. J., Motiyenko R. A., Remijan A., Guillemin J. C., Wong A., McNaughton D., 2020, A&A, 642, A206
Motiyenko R. A., Margulès L., Goubet M., Møllendal H., Konovalov A., Guillemin J.-C., 2010, The Journal of Physical Chemistry A, 114, 2794
Motiyenko R. A., Margulès L., Alekseev E. A., Guillemin J.-C., 2015, The Journal of Physical Chemistry A, 119, 1048
Motiyenko R. A., Margulès L., Senent M. L., Guillemin J.-C., 2018, The Journal of Physical Chemistry A, 122, 3163
Müller H. S. P., Thorwirth S., Roth D. A., Winnewisser G., 2001, A&A, 370, L49
Müller H. S., Schlöder F., Stutzki J., Winnewisser G., 2005, Journal of Molecular Structure, 742, 215
Müller H. S., Belloche A., Menten K. M., Comito C., Schilke P., 2008, Journal of Molecular Spectroscopy, 251, 319
Müller H. S. P., Jørgensen J. K., Guillemin J.-C., Lewen F., Schlemmer S., 2023, MNRAS, 518, 185
Ortiz-León G. N., et al., 2017, ApJ, 834, 143
Parise B., Castets A., Herbst E., Caux E., Ceccarelli C., Mukhopadhyay I., Tielens A. G. G. M., 2004, A&A, 416, 159
Persson M. V., et al., 2018, A&A, 610, A54
Pickett H. M., 1972, J. Chem. Phys., 56, 1715
Pickett H. M., 1991, Journal of Molecular Spectroscopy, 148, 371
Pickett H., Poynter R., Cohen E., Delitsky M., Pearson J., Müller H., 1998, J. Quant. Spectrosc. Radiative Transfer, 60, 883
Roueff E., Lis D. C., van der Tak F. F. S., Gerin M., Goldsmith P. F., 2005, A&A, 438, 585
Schwartz A. W., Goverde M., 1982, Journal of molecular evolution, 18, 351
Smirnov I., Alekseev E., Piddyachiy V., Ilyushin V., Motiyenko R., 2013, Journal of Molecular Spectroscopy, 293–294, 33
Vastel C., Bottinelli S., Caux E., Glorian J., Boiziot M., 2015, in SF2A-2015: Proceedings of the Annual meeting of the French Society of Astronomy and Astrophysics. pp 313–316
Wilson T. L., Rood R. T., 1994, ARA&A, 32, 191
Zakharenko O., Motiyenko R. A., Margulès L., Huet T. R., 2015, Journal of Molecular Spectroscopy, 317, 41
Zeng S., Quénard D., Jiménez-Serra I., Martí n Pintado J., Rivilla V. M., Testi L andMartí n-Domé nech R., 2019, MNRAS, 484, L43

This paper has been typeset from a TEX/LATEX file prepared by the author.

[6] https://cds.unistra.fr
[7] https://lsd.univ-lille.fr